Spin–Orbital-Angular-Momentum Coupled Bose-Einstein Condensates

H.-R. Chen,[1] K.-Y. Lin,[1] P.-K. Chen,[1] N.-C. Chiu,[1] J.-B. Wang,[1] C.-A. Chen,[1] P.-P. Huang,[1] S.-K. Yip,[1,2] Yuki Kawaguchi,[3] and Y.-J. Lin[1,*]

[1]*Institute of Atomic and Molecular Sciences, Academia Sinica, Taipei 10617, Taiwan*
[2]*Institute of Physics, Academia Sinica, Taipei 11529, Taiwan*
[3]*Department of Applied Physics, Nagoya University, Nagoya 464-8603, Japan*

(Received 1 December 2017; published 13 September 2018)

We demonstrate coupling between the atomic spin- and orbital-angular momentum (OAM) of the atom's center-of-mass motion in a Bose-Einstein condensate (BEC). The coupling is induced by Raman-dressing lasers with a Laguerre-Gaussian beam and creates coreless vortices in an $F = 1$ ^{87}Rb spinor BEC. We observe correlations between spin and OAM in the dressed state and characterize the spin texture; the result is in good agreement with the theory. In the presence of the Raman field, our dressed state is stable for 0.1 s or longer, and it decays due to collision-induced relaxation. As we turn off the Raman beams, the vortex cores in the bare spin $|m_F = 1\rangle$ and $|-1\rangle$ split. These spin-OAM coupled systems with the Raman-dressing approach have great potential for exploring new topological textures and quantum states.

DOI: 10.1103/PhysRevLett.121.113204

One of the most exciting and productive research directions for ultracold atoms has been engineering interesting Hamiltonians for creating atomic gas analogs to iconic condensed-matter models [1]. Another motivation is to create systems with fundamentally new regimes of quantum, topological, or other forms of matter with no analogs elsewhere [2]. A landmark of this theme was the creation of synthetic gauge potentials that act upon neutral atoms as if they were charged particles [3–11]. A key experimental technique for producing such synthetic gauge fields is optical Raman coupling between different internal spin states, where photon momentum is transferred to the atoms as the spin state changes. This technique leads naturally to the kind of "spin-orbit coupling" (SOC) seen in solids, where the linear momentum of electrons (atoms in our analog system) is coupled to their spin: $\hbar\vec{k}_e \cdot \vec{s}$. We refer to this as spin–linear-momentum coupling (SLMC) [11–14].

In this Letter, we develop theoretically, and demonstrate experimentally, a new kind of general SOC in which the orbital-angular-momentum (OAM) of atoms' center-of-mass couples to their internal spin state, here referred to as spin–orbital-angular-momentum coupling (SOAMC). Amusingly, SOAMC is closer to the original meaning of spin-orbit coupling in atomic physics, where the OAM of an electron in an atom couples to the electron spin. The SOAMC we report can be described by the Hamiltonian,

$$\hat{H}_0 = \hat{h}_{\hat{1}} + \hbar\delta\hat{F}_z + \hbar\Omega\hat{F}_x + \hat{H}_{\mathrm{SOAMC}} + \frac{\hbar^2}{2mr^2}\hat{F}_z^2, \quad (1)$$

where $\hat{h}_{\hat{1}} = -(\hbar^2/2m)\nabla^2(r,z) + L_z^2/2mr^2$, $\nabla^2(r,z) = r^{-1}\partial_r(r\partial_r) + \partial_z^2$, $L_z = -i\hbar\partial_\phi$ is the canonical angular momentum, $\hat{F}_i$ are the spin-1 matrices, δ and Ω are the effective magnetic fields along $\mathbf{e}_z$ and $\mathbf{e}_x$, and $\hat{H}_{\mathrm{SOAMC}} = (\hbar/mr^2)L_z\hat{F}_z$ is the SOAMC term. Here $\hat{H}_0$ arises from the laboratory Hamiltonian $\hat{H}_{\mathrm{lab}}$ after a local spin rotation (see Supplemental Material [15]), where $\hat{H}_{\mathrm{lab}} = -(\hbar^2/2m)\nabla^2 + \vec{\Omega}_{\mathrm{eff}} \cdot \vec{F}$, and $\vec{\Omega}_{\mathrm{eff}}$ is the local light-induced effective magnetic field [10] from vector light shifts.

SOAMC systems [22] with $\hat{H}_0$ have azimuthal gauge potentials $A\mathbf{e}_\phi$ owing to the coupling between $\hat{F}_z$ and $L_z = -i\hbar\partial_\phi$. The stationary Hamiltonians with $A\mathbf{e}_\phi$ are equivalent to the Hamiltonians in rotating frames, where $A\mathbf{e}_\phi$ is an effective rotation. One can study the properties at equilibrium with time-independent potentials, which is impossible for systems under mechanical rotations with imperfect cylindrical symmetries. This study differs from those where metastable superflows were investigated [23–25]. The effective rotation with SOAMC can be used to measure superfluid fractions [26] using the gauge-dependent spin population imbalance of the dressed states, which vanishes in the gauge of SLMC (see Supplemental Material [15]). The gauge of SOAMC differs from that in SLMC, allowing one to probe rotational properties under cylindrically symmetric configurations.

The engineered SOAMC also allows investigation of topological excitations [27,28] with cylindrical symmetry in spinor Bose-Einstein condensate (BECS), e.g., coreless vortices [29], Skyrmions [30], and monopoles [31]. Such spin textures can be created with SOAMC, but not with SLMC. The many-body physics in SOAMC systems is rich and worth exploring in its own right, in analogy to SLMC systems with spatially uniform Raman coupling strength

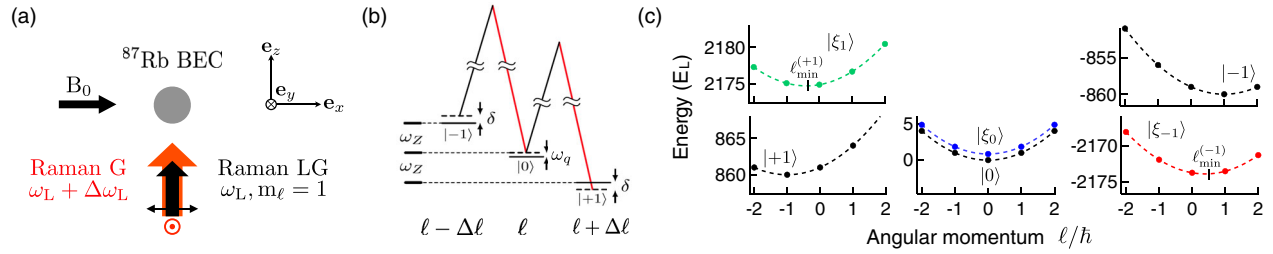

FIG. 1. (a) Experimental setup. (b) Level diagram showing the Raman beams transfer OAM $= \Delta\ell = \hbar$ between spin state $|m_F\rangle \leftrightarrow |m_F + 1\rangle$. (c) Energy dispersion $E(\ell)$ at $r = r_0 = 5$ μm without the quadratic Zeeman energy. The black symbols indicate dispersions of bare $|m_F\rangle$ without Raman coupling [see Eq. (1) and Supplemental Material [15]]. Green, blue, and red symbols represent dispersions of the dressed states $|\xi_n\rangle$ with minima at $\ell_{\min}^{(n)}(\Omega(r_0), \delta) = r_0 A_n$, which can be tuned continuously, and $n = \pm 1, 0$. Energies are in unit of $E_L = \hbar^2/2mr_0^2 = h \times 2.326$ Hz; $(\Omega(r_0), \delta) = 2\pi \times (4.6, 2.0)$ kHz.

and Raman detuning. Examples that have been discussed in SLMC include effective two-body interactions [32], related physics with optical lattices [33,34], and ground state phases with spin-dependent interactions in the small Raman coupling regime [10,11]. The last is also considered in Refs. [35–39] for SOAMC. In this Letter, we consider $\hat{H}_{\mathrm{SOAMC}}$ where only the spin component $\hat{F}_z$ is coupled, analogous to the $k_x\hat{F}_z$ in SLMC. With our technique using Laguerre-Gaussian (LG) Raman beams to induce SOAMC, it is generally possible to create more complex forms by versatile engineering of the Raman beams, such as those with non-Abelian gauge potentials [9,10].

For dressed atoms under sufficiently large atom-light coupling $\vec{\Omega}_{\mathrm{eff}} \cdot \vec{F}$, the eigenstates of the overall Hamiltonian are well approximated as the local dressed spin states, whose quantization axis is along $\vec{\Omega}_{\mathrm{eff}}$. Thus, one can employ a slowly varying position-dependent $\vec{\Omega}_{\mathrm{eff}}$ to load the atoms into the dressed spin state by adiabatic following. This is equivalent to manipulating atoms using the spin rotation method [29–31,40] with the Hamiltonian term $\vec{B} \cdot \vec{F}$, where $\vec{B}$ is a "real" magnetic field [41]. An approach utilizing a light-induced $\vec{\Omega}_{\mathrm{eff}}$ can thus allow versatile design of $\vec{\Omega}_{\mathrm{eff}}$ to study topological excitations in spinor BECs. The rich variety of order parameters in spinor BECs can accommodate various types of topological defects [27,28]. Realizations of topological excitations include those using spin rotation methods [29–31,40,42–44] and Raman pulses of LG beams [45,46]. The topological excitations in the $|\langle\vec{F}\rangle| = 1$ manifold have spin pointing along $\vec{\Omega}_{\mathrm{eff}}$, a cylindrically symmetric configuration that cannot be created by $\vec{\Omega}_{\mathrm{eff}}$ of SLMC.

We demonstrate light-induced SOAMC in atomic BECs by dressing the atoms with a pair of Raman laser beams, one of which is a LG beam carrying OAM. The beams couple atoms between different spin states while transferring OAM from the light to the atoms' center-of-mass. We adiabatically load a ^{87}Rb BEC in $|F = 1, m_F = 0\rangle$ into the $\langle\vec{F}\rangle = 0$ (polar phase [47]) Raman-dressed state with light-induced $\vec{\Omega}_{\mathrm{eff}}$, where coreless vortices [27,28] are created. Each decomposed bare spin state $|m_F\rangle$ of the dressed state has its (orbital) angular momentum correlated with m_F, indicating SOAMC. Similar spin textures were reported in Refs. [29,30] with the spin rotation method. Here we characterize the atoms' temporal evolutions with the Raman dressing field and after turning it off. We observe that the middle-energy dressed state is stable in the Raman field for $\approx$0.1 s at Raman resonance, and that its lifetime is prolonged for larger Raman detunings. When the Raman field is turned off, we observe the vortices in the bare spin $|m_F = \pm 1\rangle$ components split into half-vortices [48], after which $|1\rangle$ and $|-1\rangle$ components spatially separate.

Consider the laboratory Hamiltonian $\hat{H}_{\mathrm{lab}}$ with $\vec{\Omega}_{\mathrm{eff}} = \Omega(r)\cos\phi\mathbf{e}_x - \Omega(r)\sin\phi\mathbf{e}_y + \delta\mathbf{e}_z$ in our setup. This Hamiltonian is transformed to $\hat{H}_0$ under a local spin rotation to remove the ϕ dependence of $\vec{\Omega}_{\mathrm{eff}}$, giving rise to $\hat{H}_{\mathrm{SOAMC}}$ and $(\hbar^2/2mr^2)\hat{F}_z^2$. Consider first the atoms with no motional degree of freedom, where the dressed eigenstates [9,10,49] are exactly given by diagonalizing $\vec{\Omega}_{\mathrm{eff}} \cdot \vec{F}$ and are the dressed spin states with the quantization axis along $\vec{\Omega}_{\mathrm{eff}}(\vec{r}, t)$. We then include the motional kinetic energy $-(\hbar^2/2m)\nabla^2$ and consider a general atomic state $\langle\vec{r}|\Psi(t)\rangle = \psi(\vec{r}, t)|\xi(\vec{r}, t)\rangle$, where ψ is the external part and $|\xi\rangle$ is the (normalized) spin part of the wave function. If the "adiabatic condition" is fulfilled, the atoms can be initially prepared in a particular branch of dressed states and remain in the same state as time evolves. The adiabatic condition is satisfied by sufficiently slowly varying external parameters and small spatial gradient in both ψ and $|\xi\rangle$. More explicitly, with small spatial gradient energies compared to the gap $|\vec{\Omega}_{\mathrm{eff}}| = \Omega_{\mathrm{eff}}$ between dressed states, it is valid to take $\hat{H}_{\mathrm{SOAMC}}$, $(\hbar^2/2mr^2)\hat{F}_z^2$, and terms with ∂_r as perturbations. Thus, $\vec{\Omega}_{\mathrm{eff}} \cdot \vec{F}$ is the dominating term in the Hamiltonian.

Given the adiabatic condition for atoms in the nth dressed state, the atomic state can be expressed as $\langle\vec{r}|\Psi(t)\rangle = \psi_n(\vec{r}, t)|\xi_n(\vec{r}, t)\rangle$, where $|\xi_n(\vec{r}, t)\rangle$ are the local dressed spin states and are normalized spinor eigenstates of

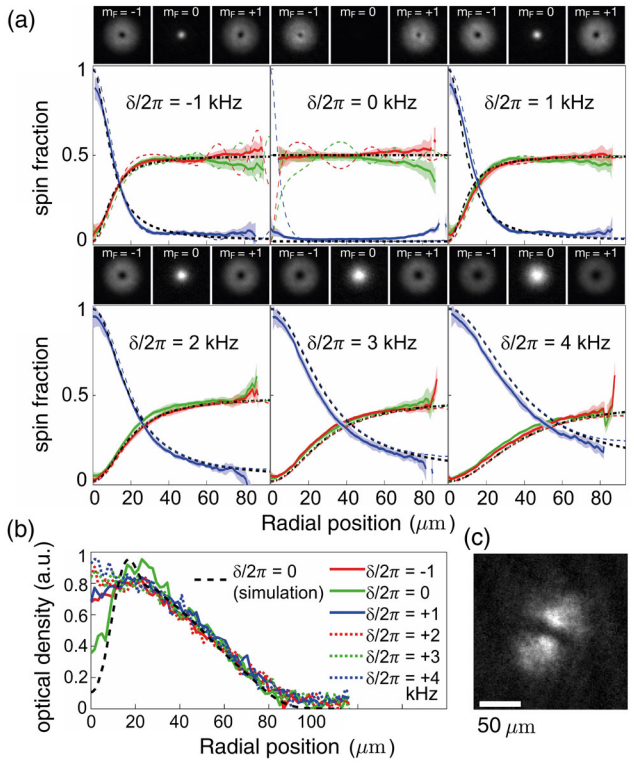

FIG. 2. Demonstration of SOAMC in the vertical images of the dressed state $|\xi_0\rangle$ after 24 ms TOF with $t_h = 1$ ms. (a) Images projected onto bare spin components $|m_F\rangle$ for $-1 < \delta/2\pi < 4$ kHz and the radial cross sections of spin textures versus theory. The image scale is 240×240 μm. The blue, red, and green curves are data for $|0\rangle, |1\rangle$, and $|-1\rangle$ components, respectively, with the shaded region indicating the uncertainty. The black dashed (dash-dotted) curves indicate predictions from Eq. (3) magnified by 9.1 in the radial position [50] for $|0\rangle(|\pm 1\rangle)$. The colored dashed curves indicate TOF simulations from 3D TDGPE. (b) Radial cross sections of the total optical density of all $|m_F\rangle$ for all δ. Colored solid and dotted (black dashed) curves denote the data (TOF simulation at $\delta = 0$). (c) Interference between $|-1\rangle$ and $|+1\rangle$ components at $\delta = 0$.

$\vec{\Omega}_{\rm eff} \cdot \vec{F}$ in states $n = 0, \pm 1$; ψ_n are the external wave functions. We then consider the projected Hamiltonian [10] $H^{(n)}_{\rm eff} = \langle \xi_n | \hat{H}_{\rm lab} | \xi_n \rangle + V(r)$, which governs the dynamic motion $\psi_n(\vec{r}, t)$ and a gauge potential $\vec{A}_n = A_n(r,t)\mathbf{e}_\phi = (i\hbar/r)\langle \xi_n | \partial_\phi \xi_n \rangle \mathbf{e}_\phi$ appears,

$$H^{(n)}_{\rm eff} = \frac{-\hbar^2}{2m}\nabla^2(r,z) + \frac{(L_z - rA_n)^2}{2mr^2} + V(r) + \varepsilon_n + W_n, \tag{2}$$

where $V(r)$ is the spin-independent trap, $\varepsilon_n = n\Omega_{\rm eff}$ is the eigenenergy of $\vec{\Omega}_{\rm eff} \cdot \vec{F}$, and W_n is the geometric scalar potential $\approx \hbar^2/2mr^2$. At sufficiently large r under the adiabatic condition, terms with ∂_r are negligible. We then consider the effective energy dispersion at fixed r versus ℓ, which is the eigenvalue of L_z quantized in units of $\hbar$. The dispersion adds up $(\ell - rA_n)^2/2mr^2$, ε_n, and W_n [Fig. 1(c)]. We label the lowest-, middle-, and highest-energy dressed states as $|\xi_{-1}\rangle$, $|\xi_0\rangle$, and $|\xi_1\rangle$, respectively. The dressed atoms in $|\xi_n\rangle$ have kinematic angular momentum $\ell - \ell^{(n)}_{\rm min}$, where $\ell^{(n)}_{\rm min} = rA_n$.

We start with a ^{87}Rb BEC in $|F = 1, m_F = -1\rangle$ state in a crossed optical dipole trap with $N \approx 4 \times 10^5$ atoms. The condensate is approximately spherical symmetric with a Thomas-Fermi (TF) radius $R_{\rm TF} \approx 10$ μm. A bias magnetic field B_0 along $\mathbf{e}_x$ gives a linear Zeeman shift $\omega_Z/2\pi = 0.57$ MHz and a quadratic Zeeman shift $\hbar\omega_q \hat{F}_z^2$ with $\omega_q/2\pi = 50$ Hz. Two $\lambda = 790$ nm Raman laser beams copropagate along $\mathbf{e}_z$. One is a Gaussian beam (G), and the other is a LG beam with phase winding $m_\ell = 1$. The Raman beams transfer OAM $= \triangle\ell = \hbar$ when coupling the atoms from $|m_F\rangle$ to $|m_F + 1\rangle$ [Figs. 1(a) and 1(b)]. The Raman laser frequencies differ by $\Delta\omega_L$, and the Raman detuning is $\delta = \Delta\omega_L - \omega_Z$. We transfer the BEC to $|m_F = 0\rangle$ and then load the atoms into the $|\xi_0\rangle$ dressed state with $\Omega(r,t)$ and $\delta(t)$. The final value of Raman coupling strength is $\Omega(r) = \Omega_M \sqrt{e}(r/r_M)e^{-r^2/2r_M^2}$, where $\Omega_M/2\pi = 10$ kHz; $r_M = 17$ μm is the radius at peak intensity. The resulting $\vec{\Omega}_{\rm eff}$ has the polar angle $\beta(r) = \tan^{-1}[\Omega(r)/\delta]$.

We load the atoms into the dressed state by turning on $\Omega(r)$ in 15 ms at detuning $\delta/2\pi = 5$ kHz, followed by ramping $\delta/2\pi$ to between 4 and -1 kHz. The resulting spinor state is the local dressed state $|\xi_0\rangle$ for $r > r_c$ where the adiabatic condition is fulfilled. Here r_c is the adiabatic radius determined by the loading speed $\dot{\delta}$ and spatial gradient energies with respect to $\Omega_{\rm eff}(r)$. The quadratic Zeeman shift is smaller than $\Omega_{\rm eff}(r)$ or spatial gradient energies; thus its effect is negligible. We perform 3D time-dependent-Gross-Pitaevskii equation (TDGPE) simulations, including the kinetic energies, quadratic Zeeman energy, and mean field interaction parameters $c_0 = 4\pi\hbar^2(a_0 + 2a_2)/3m$ and $c_2 = 4\pi\hbar^2(a_2 - a_0)/3m < 0$, where a_f is the s-wave scattering length in the total spin f channel [47]. This gives $r_c \approx 1.4$ μm at resonance $\delta = 0$.

To a good approximation, for $r > r_c$, the condensate can be loaded into the local dressed state [47]

$$|\xi_0\rangle = [-e^{i\phi}\sin\beta(r)/\sqrt{2}, \cos\beta(r), e^{-i\phi}\sin\beta(r)/\sqrt{2}]^T, \tag{3}$$

where the local quantization axis is along $\vec{\Omega}_{\rm eff}$ with $A_0 = 0$ during loading. The wave functions of bare spin $|m_F\rangle$ components possess spin-dependent angular momentum $\ell + m_F\hbar$, showing the SOAMC; here $\ell = 0$. For atoms in $|\xi_{\pm 1}\rangle$, $A_{\pm 1} = \mp(\hbar/r)\cos\beta(r)$ [see Fig. 1(c)] are the azimuthal gauge potentials.

Following the preparation, we probe the dressed state after a hold time t_h by switching off the Raman beams and dipole trap simultaneously and then adiabatically rotating the bias field to the direction along the imaging beam. After

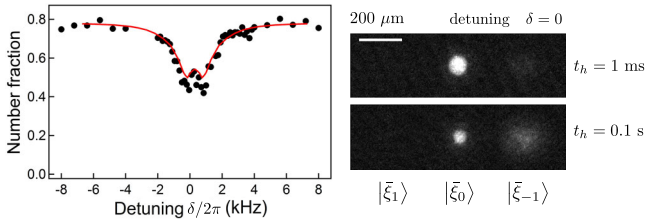

FIG. 3. Left panel: Number fraction in the dressed state $|\xi_0\rangle$ after a $t_h = 0.1$ s hold time with Raman fields on versus detuning $\delta/2\pi$, compared with that from the calculated rate (red curve). Right panel: Side images at $\delta = 0$ for $t_h = 1$ ms and 0.1 s.

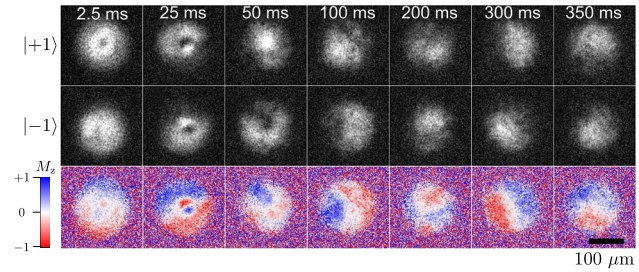

FIG. 4. Time evolution of the initially prepared dressed state at $\delta = 0$ after a sudden turn-off of the Raman fields and holding $t_{\rm off}$, $2.5 \le t_{\rm off} \le 350$ ms. The images in the top and middle row are projected to $|m_F = \pm 1\rangle$; the $|m_F = 0\rangle$ components are not discernible. The images are from single experiments and are selected to best illustrate the evolution. The bottom row shows magnetization images $M_z = (D_1 - D_{-1})/(D_1 + D_0 + D_{-1})$.

a 24 ms time of flight (TOF), we take images along the z direction of each spin m_F state, respectively, by using microwave spectroscopy for m_F-selected imaging. A single m_F state is imaged in an experimental realization. With all spin states expanding together during TOF, in the $|c_2| \approx 0$ limit each $|m_F\rangle$ after TOF approximately experiences a self-similar dilation of the *in situ* profile by the same factor [50], verified by the TDGPE simulations; the *in situ* and TOF profiles largely agree at $r \gtrsim 2$ μm. The only exception is for $\delta \lesssim 0$, where the $|\pm 1\rangle$ components show oscillations of spin imbalance versus r after TOF [Fig. 2(a)]. The images for different detuning δ with a short $t_h = 1$ ms are shown in Fig. 2(a), indicating $|0\rangle$ carries zero angular momentum and $|\pm 1\rangle$ carry the same magnitude of angular momentum from their same hole sizes. To prove $|+1\rangle$, $|-1\rangle$ carry $\pm\hbar$ (or $\mp\hbar$), we take the interference between the two components at $\delta = 0$, where the nodal line shows the 4π relative phase winding [Fig. 2(c)]. The spin-dependent angular momentum demonstrates SOAMC. Figure 2(a) shows radial cross sections of the spin texture $D_{m_F}/(D_1 + D_0 + D_{-1})$ after averaging over the azimuthal angles compared to Eq. (3) and TOF simulations, where D_{m_F} is the optical density of $|m_F\rangle$. At $\delta = 0$, the population in $|0\rangle$ reaches the minimum; at the TOF position $r_{\rm TOF} \gtrsim 9$ μm corresponding to the *in situ* $r > 1$ μm, the data do not show the predicted oscillations of spin imbalance, likely due to small dissipations in the experiment. The profile at $\delta/2\pi = 1$ kHz is similar to that at $\delta/2\pi = -1$ kHz for $r > r_c$ as expected. Our experimental results agree with the prediction for $-1 < \delta/2\pi < 4$ kHz.

We theoretically discuss the stability of the dressed atoms with the Raman field for $t_h > 0$. Without the interaction, the total Hamiltonian after the local spin rotation is $\hat{H}_1 = \hat{H}_0 + V(r)$. By neglecting terms with ∂_r, the eigenstates at fixed r with the good quantum number ℓ are the "modified local dressed states" $|\bar{\xi}_n(\ell, r)\rangle$, which deviate from $|\xi_n\rangle$ due to $L_z^2/2mr^2$ and the last two terms in Eq. (1). While at $\ell = 0$, $|\bar{\xi}_n(\ell, r)\rangle$ approximates $|\xi_n\rangle$ for $r > r_c$. With our $\dot{\delta}$, for $r \gtrsim 1.4$ μm, the atoms are adiabatically prepared in $|\xi_0\rangle \approx |\bar{\xi}_0\rangle$ at $\ell = 0$. From TDGPE simulations, we find $|\bar{\xi}_0\rangle$ is coupled to $|\bar{\xi}_{-1}\rangle$ after a hold time with $\ell = 0$ unchanged (see Supplemental Material [15]). Beyond the mean field description, we consider interactions in the second quantization form $\hat{H}_{\rm int}^{c_0}$, where the dominating spin-independent c_0 term can make the dressed atoms decay to the lowest-energy state $|\bar{\xi}_{-1}\rangle$ in the presence of general SOC [51,52]. In contrast, the c_0 term cannot couple between bare spin states.

We study the stability of the spinor state initially loaded into $|\xi_0\rangle \approx |\bar{\xi}_0\rangle$ with the Raman field. To investigate time-evolving distributions in dressed states, we perform deloading after a variable hold time t_h; for $r > r_c$, we map the dressed states $|\bar{\xi}_{-1}\rangle, |\bar{\xi}_0\rangle$, and $|\bar{\xi}_1\rangle$ back to the bare spin states $|-1\rangle, |0\rangle$, and $|+1\rangle$, respectively. We take side images after 14 ms TOF with Stern-Gerlach gradient versus δ with $t_h = 1$ ms and 0.1 s. We display the fraction of the atom number in $|\bar{\xi}_0\rangle$ over the total number in $|\bar{\xi}_0\rangle$ and $|\bar{\xi}_{-1}\rangle$ at $t_h = 0.1$ s (Fig. 3). We compare the data with the simulation of decay (see Supplemental Material [15]) from $|\bar{\xi}_0\rangle$ to $|\bar{\xi}_{-1}\rangle$ due to the collisions $\hat{H}_{\rm int}^{c_0}$, and the two agree (Fig. 3).

Finally, we investigate evolutions of the initial dressed state after turning off the Raman fields. TOF vertical images are taken after leaving the sample in the dipole trap with a hold time $t_{\rm off}$ (see Fig. 4). We observe that the $|m_F = \pm 1\rangle$ vortices repel each other, and the domains in magnetization images show spatial separation. At $t_{\rm off} \ge 50$ ms, the images vary in different experimental shots under identical conditions, likely due to variations of vortex centering in the shots and dynamical instabilities. Similar dynamics has also been studied in Ref. [30].

In conclusion, we demonstrate SOAMC by creations of coreless vortices in the $F = 1$ polar phase BEC by loading the atoms into Raman dressed states. We also study their stability with and without the Raman fields. Going beyond our initial demonstration, the transverse components of light-induced $\vec{\Omega}_{\rm eff}$ can be engineered via intensity and phase patterns of the Raman beams using spatial-light modulators, and the axial component can be manipulated via vector light shifts from another laser. Designing of $\vec{\Omega}_{\rm eff}$

enables smaller spatial scales and faster timescales than using a real magnetic field $\vec{B}$ and opens more possibilities for creating topological structures. Manipulations with $\vec{\Omega}_{\text{eff}}$, instead of $\vec{B}$, allow independent control of $\vec{B}$. With nonzero $\nabla \cdot \vec{\Omega}_{\text{eff}}$, one can create a synthetic "antimonopole" with opposite charge to that generated by $\vec{B}$ in Refs. [31]. The interaction of a monopole-antimonopole pair or a vortex pair with controlled pair sizes can be studied. With noncollinear vortices, their collisions, cutting, and reconnections can be studied. For non-Abelian vortices in the $F = 2$ manifold, the production of rung vortex [27,28] can be tested. Further, generating high-order LG Raman beams may reach larger $E_L \propto \Delta\ell^2$ and potentially access the small Raman coupling regime with multiple minima in the energy dispersion and the predicted miscible annular stripe phases [35–37] (see Supplemental Material [15]).

The authors thank M.-S. Chang, C. Chin, I.-B.Spielman, B. Xiong, and J. T. Hougen for useful discussions and W. D. Phillips for critical readings of the manuscript. We also thank H.-J. Wei and C.-Y. Yu for their contributions to build the experiment. Y.-J. L. was supported by MOST Grant No. 100-2112-M-001-027-MY3, Career Development Awards in Academia Sinica and NCTS ECP1. S.-K. Y. was supported by MOST Grant No. 104-2112-M-001-006-MY3. Y. K. was supported by JSPS KAKENHI Grants No. JP15K17726 and No. JP16H00989.

*linyj@gate.sinica.edu.tw

[1] I. Bloch, J. Dalibard, and W. Zwerger, Rev. Mod. Phys. **80**, 885 (2008).
[2] V. Galitski and I. B. Spielman, Nature (London) **494**, 49 (2013).
[3] Y.-J. Lin, R. L. Compton, A. R. Perry, W. D. Phillips, J. V. Porto, and I. B. Spielman, Phys. Rev. Lett. **102**, 130401 (2009).
[4] M. Aidelsburger, M. Atala, M. Lohse, J. T. Barreiro, B. Paredes, and I. Bloch, Phys. Rev. Lett. **111**, 185301 (2013).
[5] H. Miyake, G. A. Siviloglou, C. J. Kennedy, W. C. Burton, and W. Ketterle, Phys. Rev. Lett. **111**, 185302 (2013).
[6] J. Struck, C. Ölschläger, M. Weinberg, P. Hauke, J. Simonet, A. Eckardt, M. Lewenstein, K. Sengstock, and P. Windpassinger, Phys. Rev. Lett. **108**, 225304 (2012).
[7] C. V. Parker, L.-C. Ha, and C. Chin, Nat. Phys. **9**, 769 (2013).
[8] G. Jotzu, M. Messer, R. Desbuquois, M. Lebrat, T. Uehlinger, D. Greif, and T. Esslinger, Nature (London) **515**, 237 (2014).
[9] J. Dalibard, F. Gerbier, G. Juzeliūnas, and P. Öhberg, Rev. Mod. Phys. **83**, 1523 (2011).
[10] N. Goldman, G. Juzeliunas, P. Öhberg, and I. B. Spielman, Rep. Prog. Phys. **77**, 126401 (2014).
[11] H. Zhai, Rep. Prog. Phys. **78**, 026001 (2015).
[12] Y.-J. Lin, K. Jimenez-Garcia, and I. B. Spielman, Nature (London) **471**, 83 (2011).
[13] Z. Wu, L. Zhang, W. Sun, X.-T. Xu, B.-Z. Wang, S.-C. Ji, Y. Deng, S. Chen, X.-J. Liu, and J.-W. Pan, Science **354**, 83 (2016).
[14] L. Huang, Z. Meng, P. Wang, P. Peng, S.-L. Zhang, L. Chen, D. Li, Q. Zhou, and J. Zhang, Nat. Phys. **12**, 540 (2016).
[15] See Supplemental Material at http://link.aps.org/supplemental/10.1103/PhysRevLett.121.113204 for gauge dependence, high-order Laguerre-Gaussian beams, magnetic field control, BEC production, imaging calibration, and deloading, which includes Refs. [16–21].
[16] L. J. LeBlanc, K. Jiménez-García, R. A. Williams, M. C. Beeler, W. D. Phillips, and I. B. Spielman, New J. Phys. **17**, 065016 (2015).
[17] S. Moulder, Ph.D. thesis, University of Cambridge (2013).
[18] D. Trypogeorgos, A. Valdés-Curiel, N. Lundblad, and I. B. Spielman, Phys. Rev. A **97**, 013407 (2018).
[19] Y.-J. Lin, A. R. Perry, R. L. Compton, I. B. Spielman, and J. V. Porto, Phys. Rev. A **79**, 063631 (2009).
[20] G. Reinaudi, T. Lahaye, Z. Wang, and D. Guéry-Odelin, Opt. Lett. **32**, 3143 (2007).
[21] Y.-J. Lin, R. L. Compton, K. Jiménez-García, W. D. Phillips, J. V. Porto, and I. B. Spielman, Nat. Phys. **7**, 531 (2011).
[22] G. Juzeliunas, P. Öhberg, J. Ruseckas, and A. Klein, Phys. Rev. A **71**, 053614 (2005).
[23] A. Ramanathan, K. C. Wright, S. R. Muniz, M. Zelan, W. T. Hill, C. J. Lobb, K. Helmerson, W. D. Phillips, and G. K. Campbell, Phys. Rev. Lett. **106**, 130401 (2011).
[24] K. C. Wright, R. B. Blakestad, C. J. Lobb, W. D. Phillips, and G. K. Campbell, Phys. Rev. Lett. **110**, 025302 (2013).
[25] S. Beattie, S. Moulder, R. J. Fletcher, and Z. Hadzibabic, Phys. Rev. Lett. **110**, 025301 (2013).
[26] N. R. Cooper and Z. Hadzibabic, Phys. Rev. Lett. **104**, 030401 (2010).
[27] Y. Kawaguchi and M. Ueda, Phys. Rep. **520**, 253 (2012).
[28] M. Ueda, Rep. Prog. Phys. **77**, 122401 (2014).
[29] A. E. Leanhardt, Y. Shin, D. Kielpinski, D. E. Pritchard, and W. Ketterle, Phys. Rev. Lett. **90**, 140403 (2003).
[30] J.-Y. Choi, W. J. Kwon, and Y.-I. Shin, Phys. Rev. Lett. **108**, 035301 (2012).
[31] M. W. Ray, E. Ruokokoski, S. Kandel, M. Möttönen, and D. S. Hall, Nature (London) **505**, 657 (2014).
[32] R. A. Williams, L. J. LeBlanc, K. Jiménez-García, M. C. Beeler, A. R. Perry, W. D. Phillips, and I. B. Spielman, Science **335**, 314 (2012).
[33] W. S. Cole, S. Zhang, A. Paramekanti, and N. Trivedi, Phys. Rev. Lett. **109**, 085302 (2012).
[34] J. Radić, A. Di Ciolo, K. Sun, and V. Galitski, Phys. Rev. Lett. **109**, 085303 (2012).
[35] C. Qu, K. Sun, and C. Zhang, Phys. Rev. A **91**, 053630 (2015).
[36] K. Sun, C. Qu, and C. Zhang, Phys. Rev. A **91**, 063627 (2015).
[37] L. Chen, H. Pu, and Y. Zhang, Phys. Rev. A **93**, 013629 (2016).
[38] M. DeMarco and H. Pu, Phys. Rev. A **91**, 033630 (2015).
[39] Y.-X. Hu, C. Miniatura, and B. Grémaud, Phys. Rev. A **92**, 033615 (2015).
[40] T. Ollikainen, K. Tiurev, A. Blinova, W. Lee, D. S. Hall, and M. Möttönen, Phys. Rev. X **7**, 021023 (2017).

[41] T. Isoshima, M. Nakahara, T. Ohmi, and K. Machida, Phys. Rev. A **61**, 063610 (2000).
[42] J.-Y. Choi, W. J. Kwon, M. Lee, H. Jeong, K. An, and Y.-I. Shin, New J. Phys. **14**, 053013 (2012).
[43] M. W. Ray, E. Ruokokoski, K. Tiurev, M. Möttönen, and D. S. Hall, Science **348**, 544 (2015).
[44] D. S. Hall, M. W. Ray, K. Tiurev, E. Ruokokoski, A. H. Gheorghe, and M. Möttönen, Nat. Phys. **12**, 478 (2016).
[45] K. C. Wright, L. S. Leslie, A. Hansen, and N. P. Bigelow, Phys. Rev. Lett. **102**, 030405 (2009).
[46] L. S. Leslie, A. Hansen, K. C. Wright, B. M. Deutsch, and N. P. Bigelow, Phys. Rev. Lett. **103**, 250401 (2009).
[47] T.-L. Ho, Phys. Rev. Lett. **81**, 742 (1998).
[48] S. W. Seo, W. J. Kwon, S. Kang, and Y. Shin, Phys. Rev. Lett. **116**, 185301 (2016).
[49] I. B. Spielman, in *Annual Review of Cold Atoms and Molecules* (World Scientific, Singapore, 2013), p. 145.
[50] Y. Castin and R. Dum, Phys. Rev. Lett. **77**, 5315 (1996).
[51] I. B. Spielman, Phys. Rev. A **79**, 063613 (2009).
[52] L. Zhang, J.-Y. Zhang, S.-C. Ji, Z.-D. Du, H. Zhai, Y. Deng, S. Chen, P. Zhang, and J.-W. Pan, Phys. Rev. A **87**, 011601 (2013).